# The decay of swirl in a pipe

**M. J. Reader-Harris**
National Engineering Laboratory, East Kilbride, Scotland

The way in which swirling flow in a pipe decays has been computed by solving an approximation to the Navier–Stokes equations. The approximation was performed using an order-of-magnitude analysis and a turbulent viscosity that is computed as part of the solution. At a sufficient distance downstream of a swirl-inducing fitting, the flow is predicted to rotate approximately as a solid body: experimental data confirm this prediction. Swirl decay rates have been computed and found to be very nearly proportional to pipe friction factor: this result is also in good agreement with experiment and implies that swirl is extremely persistent in smooth pipes at high Reynolds numbers.

**Keywords:** swirling flow; pipe flow

## Introduction

The decay of swirling flow in a pipe is of great importance. For example, since swirl can cause significant errors in flow measurement, it is important to know what length of straight pipe is required for a given upstream swirl to reduce to a specified acceptable level of swirl. The international standard ISO 5167-1 (1991) for flow measurement using orifice plates, nozzles, and Venturi tubes requires that, where specific installation conditions cannot be met, the swirl angle must be measured and must be less than 2° over the pipe.

In a key paper, Kreith and Sonju (1965) computed the decay of swirl by solving an approximation to the Navier–Stokes equations. Their approximation was performed using an order-of-magnitude analysis and the assumption of a constant turbulent viscosity. In their comparison of the computed swirl velocity distribution with the experimental measurements of Musolf (1963), they found good agreement at distances less than 20 diameters downstream of a twisted-tape swirl inducer, but deviations further downstream. Their computational work predicts that downstream of a substantial length of straight pipe, the maximum circumferential velocity should be roughly halfway between the center of the pipe and the wall. However, in the experimental measurements of Musolf (1993) downstream of the inducer and of both Mattingly and Yeh (1990) and Mottram and Rawat (1986) downstream of two bends in perpendicular planes, the flow rotates approximately as a solid body even quite a short distance downstream of the disturbance, and the maximum circumferential velocity is obtained quite near the pipe wall.

It is worth noting that in the case of a very strongly swirling flow (with a maximum swirl angle of about 60°) produced by an axial flow type impeller by Murakami et al. (1976), the flow eventually rotates as a solid body. The location of the maximum circumferential velocity is initially at 65% of the distance from the axis to the pipe wall; as the flow moves downstream, a free-vortex-type flow is established, and the maximum moves towards the axis to about 35% of the distance from axis to wall at minimum, and then back towards the pipe wall. At a maximum swirl angle of about 14°, the maximum circumferential velocity is located very close to the wall, and at a maximum swirl angle of about 9° the flow rotates as a solid body.

In order to resolve the discrepancy between computation and experiment, computational work has been undertaken at the National Engineering Laboratory (NEL) in Scotland. The simplified circumferential momentum equation derived by Kreith and Sonju (1965) is retained; however, the turbulent viscosity is no longer constant, but calculated from the axial momentum equation. In this case the computed flow does indeed rotate approximately as a solid body. Moreover, good agreement with experimentally measured swirl decay rates is obtained.

The use of the turbulent viscosity derived from the axial momentum equation in the circumferential momentum equation is based on the assumption that, although in swirling flow in general the turbulent viscosity is anisotropic, in weak swirl (after a sufficient length of straight pipe) the turbulent viscosity may be considered isotropic because the circumferential velocity is small. Even in strong swirl in a straight pipe the anisotropy is weak close to the wall (Kitoh 1991). Whereas Kreith and Sonju did not need to assume that the turbulent viscosity is isotropic, their method involved introducing its value in the circumferential momentum equation from experimental measurements. However, if the swirl is weak and the turbulent viscosity is assumed anisotropic, it is very difficult to obtain a measured value for the circumferential turbulent viscosity. Moreover, the turbulent viscosity used here has more appropriate behavior near the pipe wall than the constant value used previously.

## Deriving the governing equations

For steady, incompressible, axisymmetric, turbulent flow, the time-averaged equations of conservation of mass and of momentum in cylindrical polar coordinates are as follows:

$$\frac{\partial U}{\partial x} + \frac{1}{r}\frac{\partial (rV)}{\partial r} = 0 \tag{1}$$

$$U\frac{\partial U}{\partial x} + V\frac{\partial U}{\partial r} = -\frac{1}{\rho}\frac{\partial P}{\partial x} + \nu\left(\frac{\partial^2 U}{\partial x^2} + \frac{\partial^2 U}{\partial r^2} + \frac{1}{r}\frac{\partial U}{\partial r}\right) - \left(\frac{\partial}{\partial x}\overline{u'^2} + \frac{1}{r}\frac{\partial}{\partial r} r\overline{u'v'}\right) \tag{2}$$

Address reprint requests to Dr. Reader-Harris at the National Engineering Laboratory, East Kilbride, Glasgow G75 0QU, Scotland.

Received 25 November 1993; accepted 23 December 1993

$$U\frac{\partial V}{\partial x}+V\frac{\partial V}{\partial r}-\frac{W^2}{r}=-\frac{1}{\rho}\frac{\partial P}{\partial r}+\nu\left(\frac{\partial^2 V}{\partial x^2}+\frac{\partial^2 V}{\partial r^2}+\frac{1}{r}\frac{\partial V}{\partial r}-\frac{V}{r^2}\right)-\left(\frac{\partial}{\partial x}\overline{u'v'}+\frac{1}{r}\frac{\partial}{\partial r}r\overline{v'^2}-\frac{\overline{w'^2}}{r}\right) \quad (3)$$

$$U\frac{\partial W}{\partial x}+V\frac{\partial W}{\partial r}+\frac{VW}{r}=\nu\left(\frac{\partial^2 W}{\partial x^2}+\frac{\partial^2 W}{\partial r^2}+\frac{1}{r}\frac{\partial W}{\partial r}-\frac{W}{r^2}\right)-\left(\frac{\partial}{\partial x}\overline{u'w'}+\frac{\partial}{\partial r}\overline{v'w'}+2\frac{\overline{v'w'}}{r}\right) \quad (4)$$

where $U$, $V$, and $W$ are the mean and $u'$, $v'$, and $w'$ the fluctuating velocity components in the axial, radial, and circumferential directions, respectively, and $x$ and $r$ are the axial and radial coordinates. $P$ is the mean pressure at a point, $\rho$ is the density, and $\nu$ is the kinematic viscosity. The bar over a function of fluctuating quantities denotes its time-averaged value.

In order to solve these equations, it is necessary first to use order-of-magnitude analysis. The essential assumption made is that the circumferential velocity is small compared with the mean axial velocity. Then

$$\left.\begin{aligned} r &= Rs \\ x &= 2Dz/\lambda \\ U &= \bar{U}\{u(s)+\delta u_1(s,z)\} \\ W &= \gamma\bar{U}w \\ P &= \rho\bar{U}^2 p \end{aligned}\right\} \quad (5)$$

where $R$ is the pipe radius, $D$ is its diameter, $\bar{U}$ is the pipe mean axial velocity, $\lambda$ is the pipe friction factor (defined in Schlichting 1960), and $\gamma$ and $\delta$ are small.

This nondimensionalization of $x$ expresses the very different length scales in the axial and radial directions (since $\lambda/4$ is very small) and is appropriate because, in a nonswirling flow, $\partial p/\partial z = -1$ from the definition of $\lambda$. $u(s)$ is the fully developed velocity profile. Then considering Equation 1, $V$ can reasonably be nondimensionalized as

$$V = \lambda\delta\bar{U}v/4 \quad (6)$$

The Reynolds stresses are expressed in terms of a turbulent kinematic viscosity, $\nu_T$, expressed in nondimensional terms as

$$\nu_T = \frac{\lambda}{4}\bar{U}RN_T(s) + \text{smaller terms} \quad (7)$$

and the Reynolds number is defined as

$$\mathrm{Re} = \frac{D\bar{U}}{\nu}$$

On nondimensionalizing and dropping smaller terms, Equations 2, 3, and 4 become, respectively,

$$0 = -\frac{\partial p}{\partial z}+\frac{1}{s}\frac{d}{ds}\left\{s\left(N_T+\frac{8}{\lambda\mathrm{Re}}\right)\frac{du}{ds}\right\} \quad (8)$$

$$0 = -\frac{\partial p}{\partial s} \quad (9)$$

$$u\frac{\partial w}{\partial z}=\frac{1}{s^2}\frac{\partial}{\partial s}\left\{s^2\left(N_T+\frac{8}{\lambda\mathrm{Re}}\right)\left(\frac{\partial w}{\partial s}-\frac{w}{s}\right)\right\} \quad (10)$$

Since Equation 9 implies that $p$ is a function of $z$ alone, Equation 8 implies that $\partial p/\partial z$ is in fact a constant, which must be $-1$, its value when the swirl has decayed away completely. So Equation 8 becomes

$$-1=\frac{1}{s}\frac{d}{ds}\left\{s\left(N_T+\frac{8}{\lambda\mathrm{Re}}\right)\frac{du}{ds}\right\}$$

which by integration becomes

$$-\tfrac{1}{2}s=\left(N_T+\frac{8}{\lambda\mathrm{Re}}\right)\frac{du}{ds} \quad (11)$$

Equation 10 can be solved by separation of variables. Writing $w = Z(z)S(s)$ gives

$$\frac{Z'}{Z}=\frac{1}{us^2S}\frac{d}{ds}\left\{s^2\left(N_T+\frac{8}{\lambda\mathrm{Re}}\right)\left(S'-\frac{S}{s}\right)\right\} = \text{constant} = -\phi^2 \quad (12)$$

## Notation

| | |
|---|---|
| $B$ | Roughness function |
| $D$ | Pipe diameter |
| $J_1$ | Bessel function of first order |
| $k$ | Roughness as on the Moody diagram |
| $k_s$ | Sand roughness |
| $N_R$ | Reynolds number based on pipe radius and maximum axial velocity |
| $N_T$ | Nondimensionalized turbulent kinematic viscosity |
| $P$ | Mean pressure at a point |
| $p$ | Nondimensionalized pressure |
| $R$ | Pipe radius |
| $R_a$ | Mean absolute roughness height |
| Re | Pipe Reynolds number |
| $U, V, W$ | Mean velocity components in axial, radial, and circumferential directions |
| $u', v', w'$ | Fluctuating velocity components in axial, radial, and circumferential directions |
| $\bar{U}$ | Pipe mean velocity |
| $u, u_1$ | Nondimensionalized axial velocity: fully developed and perturbation |
| $u^+, y^+$ | Axial velocity and distance from the wall, nondimensionalized using the friction velocity $\{= \bar{U}(\lambda/8)^{1/2}\}$. |
| $v, w$ | Nondimensionalized velocity components in radial and circumferential directions |
| $x, r$ | Axial and radial coordinates |
| $y$ | $S/s$ |
| $Z, S$ | Dependence of $w$ on $z$ and $s$ |
| $z, s$ | Nondimensionalized axial and radial coordinates |

*Greek symbols*

| | |
|---|---|
| $\beta$ | Decay rate |
| $\gamma, \delta$ | Small parameters |
| $\theta$ | Swirl angle |
| $\kappa_n$ | Zero of $J_1$ |
| $\lambda$ | Friction factor |
| $\nu$ | Kinematic viscosity |
| $\nu_T$ | Turbulent kinematic viscosity |
| $\rho$ | Density |
| $\phi^2$ | Eigenvalue |

*Subscripts*

| | |
|---|---|
| 1, 2, 3 | Refer to the eigenvalues and eigenvectors |

So

$$Z = \exp(-\phi^2 z) \tag{13}$$

and

$$\frac{d}{ds}\left\{s^3\left(N_T + \frac{8}{\lambda \mathrm{Re}}\right)\frac{d}{ds}\left(\frac{S}{s}\right)\right\} + \phi^2 s^3 u\left(\frac{S}{s}\right) = 0 \tag{14}$$

with boundary conditions $S(0) = S(1) = 0$. The main task is to determine the eigenvalues and eigenfunctions of Equation 14.

## Solving the swirl equation

### Constant turbulent viscosity

Kreith and Sonju (1965) assumed that $\nu_T$ (in this section relating only to the Reynolds stress term $\overline{v'w'}$) was not a function of $s$, but could be expressed simply as

$$\nu_T/\nu = 0.004\ 15 N_R^{0.86} \tag{15}$$

where $N_R$ is the pipe Reynolds number based on pipe radius and maximum axial velocity.

With the assumption of a constant turbulent viscosity, it is possible to rearrange Equations 13 and 14, respectively, as

$$Z = \exp\left\{-\kappa^2\left(N_T + \frac{8}{\lambda \mathrm{Re}}\right)z\right\} \tag{16}$$

$$\frac{d}{ds}\left\{s^3\frac{d}{ds}\left(\frac{S}{s}\right)\right\} + \kappa^2 s^3 u\left(\frac{S}{s}\right) = 0 \tag{17}$$

Moreover, if $u \equiv 1$, the solution to Equation 17 is a first-order Bessel function, and, substituting from Equation 15, the complete solution to Equations 16 and 17 is obtained:

$$w = \sum_{n=1}^{\infty} A_n J_1(\kappa_n s) \exp\left\{-\kappa_n^2(0.004\ 15 N_R^{0.86} + 1)\frac{4}{\mathrm{Re}}\frac{x}{D}\right\} \tag{18}$$

where $\kappa_n$ are the zeros of $J_1$.

For sufficiently large $x$, only the first term of this series is important: for this term, $\kappa_1 = 3.8317$, and for a given value of $x$, the maximum value of $w$ occurs at $s = 0.480\ 51$.

If a more physically realistic equation for axial velocity, $u = 60(1 - s)^{1/7}/49$, is included, then the solution to Equation 17 is a double sum of Bessel functions; the details will be found in Kreith and Sonju (1965). The complete solution to Equations 16 and 17 is a small perturbation to that for $u \equiv 1$; a more accurate equation for $u$ makes surprisingly little difference to the circumferential velocity profile.

### Computed turbulent viscosity

A more consistent approach than to use an assumed constant turbulent viscosity is to determine the turbulent viscosity from Equation 11 and substitute it into Equation 14. Writing $y = S/s$ gives

$$\frac{d}{ds}\left(-\frac{\frac{1}{2}s^4\frac{dy}{ds}}{\frac{du}{ds}}\right) + \phi^2 s^3 u y = 0 \tag{19}$$

This is in Sturm–Liouville form and has to be solved over the interval from 0 to 1 with the boundary conditions $y \to$ constant as $s \to 0$ and $y(1) = 0$. It remains to prescribe $u$: in smooth pipe,

$$u^+ = \begin{cases} y^+ & y^+ \le 5 \\ y^+ - 0.1285(y^+ - 5)^{1.5} & 5 < y^+ \le 27.19 \\ 2.5 \ln y^+ + 5.5 & 27.19 < y^+ \text{ and } 0.0390 < s \\ 5.551 - 33.3s^2 + 2.5 \ln(0.1699\ \mathrm{Re}\lambda^{1/2}) & s \le 0.0390 \end{cases} \tag{20}$$

and in rough pipe,

$$u^+ = \begin{cases} 2.5 \ln\left(\frac{1-s}{2(k_s/D)}\right) + B & 0.0390 < s \\ 0.051 - 33.3s^2 + 2.5 \ln\left(\frac{0.4805}{k_s/D}\right) + B & s \le 0.0390 \end{cases} \tag{21}$$

where $u = u^+(\lambda/8)^{1/2}$, $y^+ = 0.5(1 - s)\mathrm{Re}(\lambda/8)^{1/2}$, and $k_s$ is the sand roughness.

Values of $B$ are given in Schlichting (1960); in the completely rough regime, $B = 8.5$.

These formulations of $u$ were chosen to give good agreement with the standard formulas given in Schlichting, but with small modifications: $u$ is prescribed near the pipe axis in such a way that $du/ds = 0$ on the axis, since otherwise it is not always possible to obtain a solution to Equation 19 that satisfies its boundary conditions; in the case of the smooth pipe, a transition zone is included between the sublayer and the log-layer so that both $u$ and $du/ds$ (and thus the turbulent viscosity) are continuous for all $s$.

Since the pipe pressure gradient is proportional to the square of the mean pipe velocity, it is very important that the flow rate given by integration should be consistent with the nondimensionalization: hence,

$$2\int_0^1 us\,ds = 1 \tag{22}$$

This determines the value of $\lambda$ (although it is only possible to obtain the integral approximately if the pipe is very rough). In most cases where computed values are presented in the figures and tables, the absolute value of the difference between the value of $\lambda$ obtained using Equation 22 and that obtained using the Colebrook–White equation (quoted by Schlichting) is less than 0.0002: where $\mathrm{Re} = 10^4$, the difference is 0.0011, but the difference between the value of $\lambda$ obtained using Equation 22 and that using the Blasius equation also in Schlichting is only 0.0003; in the case of the two rough pipes, the Colebrook–White equation is not valid, since it is not valid for sand-roughened pipes in the transition regime. With the values of $u$ given in Equations 20 and 21, Equation 19 is solved for $y$ using the Nag routine D02KEF (1988). Eigenvalues, $\phi_n^2 (n = 1, 2, \ldots)$, are obtained together with corresponding eigenvectors, $y_n$. Calculations were performed first for smooth pipes at Reynolds numbers of $10^4$, $10^5$, $10^6$, and $10^7$. From the eigenvalues the decay rates, $\beta_i$, (nondimensionalized with pipe diameter; so $w \propto \exp(-\beta_i x/D)$) are obtained: $\beta_i = \lambda\phi_i^2/2$. These rates are tabulated in Table 1. In each case, the second eigenvalue is of the order of ten times the first one; so provided that the swirl angle is not too large, the circumferential velocity profile will rapidly acquire the shape of the first eigenfunction. The values of $sy_1 (= S_1$, the circumferential velocity profile) and of $sy_1/u$ (which is proportional to the tangent of the swirl angle and thus approximately to the swirl angle, $\theta$, for small swirl)

**Table 1** Swirl decay rates

| Turbulent viscosity | Pipework/profile | Re | $\lambda$ | Decay rates $\beta_1$ | $\beta_2$ | $\beta_3$ |
|---|---|---|---|---|---|---|
| $N_T$ from Equation 11 | Hydraulically smooth | $10^4$ | 0.0320 | 0.0328 | 0.313 | 0.698 |
| $N_T$ from Equation 11 | Hydraulically smooth | $10^5$ | 0.0179 | 0.0192 | 0.221 | 0.498 |
| $N_T$ from Equation 11 | Hydraulically smooth | $10^6$ | 0.0115 | 0.0123 | 0.172 | 0.391 |
| $N_T$ from Equation 11 | Hydraulically smooth | $10^7$ | 0.0080 | 0.0085 | 0.140 | 0.322 |
| $N_T$ from Equation 11 | Rough: $k_s/D = 0.003$ | $10^5$ | 0.0236 | 0.0255 | 0.259 | 0.578 |
| $N_T$ from Equation 11 | Rough: $k_s/D = 0.01$ | $10^5$ | 0.0385 | 0.0414 | 0.345 | 0.761 |
| $\nu_T$ from Equation 15 (assuming $N_R$ = Re/2) (Kreith and Sonju) | $u \equiv 1$ | $10^5$ | | 0.0274 | 0.092 | 0.193 |
| $\nu_T$ from Equation 15 (assuming $N_R$ = 30 Re/49) (Kreith and Sonju) | $u = 60(1 - s)^{1/7}/49$ | $10^5$ | | 0.0300 | 0.101 | 0.213 |

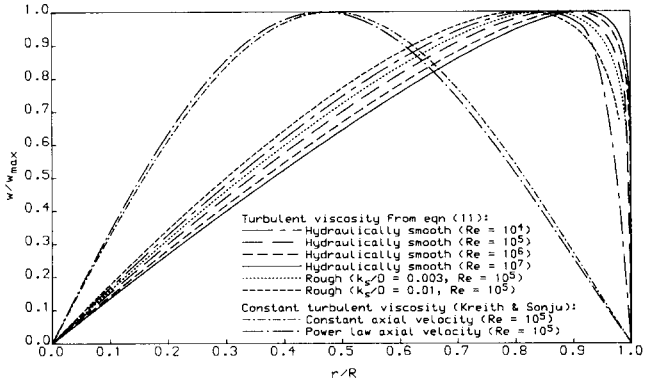


*Figure 1* Computed circumferential velocity profile

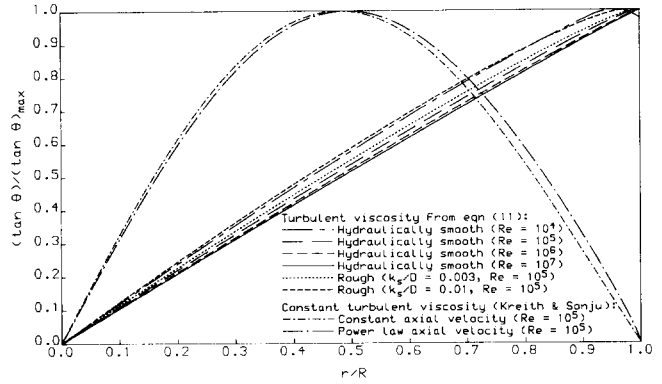


*Figure 2* Computed swirl angle profile

are given in Figures 1 and 2, respectively. Although $u$ falls rapidly to 0 as the wall is approached, $y_1/u$ remains approximately constant ($y_2/u$ and $y_3/u$ also remain approximately constant). With the assumption that in the immediate neighborhood of the wall, $y \propto u$ for rough pipe also, calculations are performed for two rough pipes, and the results are included in Table 1 and in Figures 1 and 2. For comparison, calculations using the constant turbulent viscosity assumed by Kreith and Sonju (1965) are included.

Since $\beta_2$ is so much larger than $\beta_1$, the decay rate tends very rapidly to $\beta_1$. Moreover, $\beta_1$ is well approximated by 1.07 $\lambda$, and in the cases considered in Table 1 never differs from 1.07 $\lambda$ by more than 0.012 $\lambda$, except in the case where Re = $10^4$, in which the difference is 0.04 $\lambda$. The general equation for swirl decay is thus

$$w \propto \exp(-\beta x/D),$$

where the decay rate, $\beta$, is given by

$$\beta = 1.07\,\lambda. \tag{23}$$

## Comparison with experimental data

Equation 23 can be validated by considering experimental data on swirl decay. Decay rates are presented in Baker and Sayre (1974), Kitoh (1991), Mattingly and Yeh (1990), McManus et al. (1985), and Murakami et al. (1976) and can easily be calculated from the data of Kreith and Sonju (1965), Mottram and Rawat (1986), and Senoo and Nagata (1972). Where an experimenter provided several sets of data in the same pipe at the same Reynolds number, but with differential initial swirl levels, the decay rates were almost unaffected by the initial swirl level and have been averaged. Where the decay rate changes as the swirl decays, an overall decay rate covering decay from strong swirl to weak swirl has been calculated. The friction factor of the pipe in which the data were taken was measured by Baker and Sayre and by Mottram and Rawat. The relative roughness of the pipe was measured by Mattingly and Yeh, Murakami et al., and Senoo and Nagata, and $\lambda$ can be calculated using the Colebrook–White equation. For the data of McManus et al., a pipe roughness, $k$, of 12 $\mu$m (corresponding to $R_a$ = 150 $\mu$inch, a typical value for pipe used in flow measurement) was assumed; since Kreith and Sonju used plastic pipe and their Reynolds number did not exceed $10^5$, their pipe was assumed to be hydraulically smooth. Kitoh's pipe also was hydraulically smooth. Experimental data can, therefore, be compared in Figure 3 with Equation 23 based on computation. The agreement is remarkably good, especially since the computational theory only applies for weakly swirling flow, whereas for some of the data sets the circumferential velocity even exceeded the pipe mean axial velocity. The two data points that are worst fitted are for very rough pipes, for which the values of $k/D$ were 0.008 and 0.017.

The greatest test for the computation is to compare the computed circumferential velocity and swirl angle profiles with those measured experimentally. Since the theory only applies in cases where the swirl angle is small, data with a maximum swirl angle greater than 15° are excluded from the comparison.

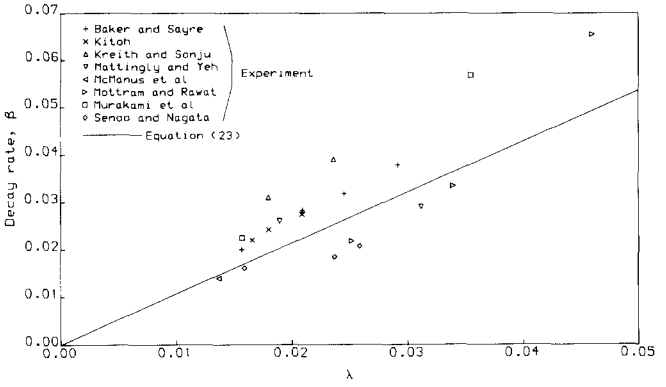


*Figure 3* Swirl decay rate

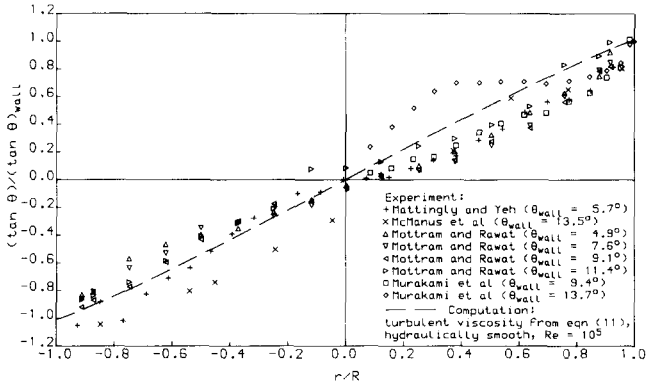


*Figure 4* Swirl angle profile: computation and experiment

Measurements of swirl angle have been presented by Mattingly and Yeh (1990), McManus et al. (1985), and Mottram and Rawat (1986); swirl angles can be calculated from the velocity profile measurements of Murakami et al. (1976). In each case, the swirl angle profiles are scaled by the swirl angle at the wall, which is obtained by extrapolation from swirl angles near the wall and by taking the mean of the wall swirl angles on two radii if a complete diameter was measured. The swirl angle profiles are presented in Figure 4. If the swirl angle at the wall is less than 3°, the data are not plotted, since it is inappropriate to scale the data by a very small angle. In the case of Mottram and Rawat (1986), only the smooth pipe data are plotted; their rough pipe data are not dissimilar. The computed swirl angle profile for a hydraulically smooth pipe with $Re = 10^5$ is also plotted in Figure 4. The agreement between the different experimental data and between the experimental data and the computation is striking, especially since the swirl was generated in many different ways: two bends in perpendicular planes, a single bend downstream of the shell side of a shell-and-tube steam heat exchanger, and an axial-flow-type impeller were used. Moreover, in some cases the flow was initially asymmetric, but the asymmetry has decayed much more rapidly than the swirl. In each case, after a sufficient distance, the swirl profile is in good agreement with that expected from the axisymmetric computation.

On the assumption of solid-body rotation, Mottram and Rawat (1986) derived a swirl decay rate similar to, but more complicated than, Equation 23. This work provides support for the main assumption made in deriving their decay rate.

It is interesting to note how small the decay rate is for smooth pipes at high Reynolds number and thus how much pipe is required for swirl induced by a fitting to decay to a level sufficiently small for accurate flow measurement. For instance, the number of diameters required for an 18° swirl immediately downstream of two bends in perpendicular planes to decay to 2° (a reduction in circumferential velocity by a factor $(\tan 2°)/(\tan 18°) = 0.1075$) is given in Table 2 for each of the combinations of roughness and Reynolds number used in Table 1. The required number of diameters varies from 65 to 261 in smooth pipes. The lengths required for swirl to decay are so large that if swirl is present, a flow straightener should be used to remove it. Even flow straighteners that have a small head loss remove swirl effectively. The remaining asymmetry decays much faster than swirl would.

## Conclusions

The way in which swirling flow decays in a pipe has been computed by solving the Navier–Stokes equations, simplified by using an order-of-magnitude analysis. The circumferential momentum equation is solved using the turbulent viscosity deduced from the axial momentum equation. At a sufficient distance downstream of a swirl-inducing fitting, the flow is predicted to rotate approximately as a solid body; experimental data confirm this prediction. Swirl decay rates have been predicted and a simple equation derived: this equation is also in good agreement with experiments. Since the swirl decay rate is approximately proportional to pipe friction factor, swirl will be extremely persistent in smooth pipes at high Reynolds numbers, and so if swirl is present, flow straighteners will probably be required for accurate flow measurement.

## Acknowledgment

This paper is published by permission of the Chief Executive, National Engineering Laboratory Executive Agency, and is Crown copyright. The work reported here was supported by the Standards, Quality and Measurement Advisory Committee and the National Measurement System Policy Unit of the Department of Trade and Industry.

**Table 2** Straight pipe required for swirl reduction to 10.75% of its initial value

| Turbulent viscosity | Pipework/profile | Re | $\lambda$ | Diameters of straight pipe |
|---|---|---|---|---|
| $N_T$ from Equation 11 | Hydraulically smooth | $10^4$ | 0.0320 | 65 |
| $N_T$ from Equation 11 | Hydraulically smooth | $10^5$ | 0.0179 | 116 |
| $N_T$ from Equation 11 | Hydraulically smooth | $10^6$ | 0.0115 | 181 |
| $N_T$ from Equation 11 | Hydraulically smooth | $10^7$ | 0.0080 | 261 |
| $N_T$ from Equation 11 | Rough: $k_s/D = 0.003$ | $10^5$ | 0.0236 | 88 |
| $N_T$ from Equation 11 | Rough: $k_s/D = 0.01$ | $10^5$ | 0.0385 | 54 |

## References


Baker, D. W. and Sayre, C. K. Jr. 1974. Decay of swirling turbulent flow of incompressible fluids in long pipes. *Flow—Its Measurement and Control in Science and Industry*, R. Dowdell (Ed.), Vol. 1. Instrument Society of America, Research Triangle Park, NC, 301–312

International Organization for Standardization. 1991. ISO 5167-1. Measurement of fluid flow by means of orifice plates, nozzles and Venturi tubes inserted in circular cross-section conduits running full. International Organization for Standardization, Geneva

Kitoh, D. 1991. Experimental study of turbulent swirling flow in a straight pipe. *J. Fluid Mech.*, **225**, 445–479

Kreith, F. and Sonju, O. K. 1965. The decay of a turbulent swirl in a pipe. *J. Fluid Mech.*, **22**, 257–271

Mattingly, G. E. and Yeh, T. T. 1990. Effects of pipe elbows and tube bundles on 50 mm orifice meters. *Proc. Semin. Installation Effects on Flow Metering* (paper 3.1). NEL, East Kilbride, Glasgow

McManus, S. E., Bateman, B. R., Brennan, J. A., Vazquez Pantoja, I., and Mann, D. 1985. The decay of swirling gas flow in long pipes. *Proc. Am. Gas Assoc. Operating Section Distribution/Transmission Conf.*, Boston, MA, American Gas Association, Arlington, VA, 629–633

Mottram, R. C. and Rawat, M. S. 1986. The swirl damping properties of pipe roughness and the implications for orifice meter installation. *Proc. Int. Conf. Flow Measurement in the Mid-80's* (Vol. 2, paper 6.1). NEL, East Kilbride, Glasgow

Murakami, M., Kito, O., Katayama, Y., and Iida, Y. 1976. An experimental study of swirling flow in pipes. *Bull. JSME*, **19**, 118–126

Musolf, A. O. 1963. An experimental investigation of the decay of turbulent swirl flow in a pipe. M.Sc. thesis, Dept. of Civil Engineering, University of Colorado, Boulder, CO

Nag Fortran Library Manual Mark 13. 1988. Numerical Algorithms Group Ltd, Oxford

Schlichting, H. 1960. *Boundary Layer Theory*. McGraw-Hill, New York

Senoo, Y. and Nagata, T. 1972. Swirl flow in long pipes with different roughness. *Bull. JSME*, **15**, 1514–1521